Biodegradation Mechanisms of Iron Oxide Monocrystalline Nanoflowers and Tunable Shield Effect of Gold Coating

Yasir Javed, Lénaic Lartigue, Pierre Hugounenq, Quoc Lam Vuong, Yves Gossuin, Rana Bazzi, Claire Wilhelm, Christian Ricolleau, Florence Gazeau, Damien Alloyeau

Small

Biodegradation mechanisms of iron oxide monocrystalline nanoflowers and tunable shield effect of gold coating

--Manuscript Draft--

Manuscript Number:	smll.201400281R2
Full Title:	Biodegradation mechanisms of iron oxide monocrystalline nanoflowers and tunable shield effect of gold coating
Article Type:	Full Paper
Section/Category:	
Keywords:	iron oxide nanoparticles, biodegradation, magnetic resonance imaging, hyperthermia, gold shell
Corresponding Author:	Damien Alloyeau Univerisité Paris Diderot Paris Cedex 13, FRANCE
Additional Information:	
Question	**Response**
Please submit a plain text version of your cover letter here. **If you are submitting a revision of your manuscript, please do not overwrite your original cover letter. There is an opportunity for you to provide your responses to the reviewers later; please do not add them here**.	Dear editor, We are pleased to submit the manuscript entitled: Biodegradation mechanism of iron oxide monocrystalline nanoflowers and tunable shield effect of gold coating, for consideration for publication in Small. Given the growing use of nanomaterials in daily life products and their many promising applications in biomedicine, humans are expected to be increasingly exposed to nano-objects. Consequently, many research efforts are presently focused on the life cycle and toxicity of nano-sized materials. However, the emerging field of nanotoxicity must be considered from different angles. While most toxicology studies warn about the effects of nanomaterials on biological functions (cytotoxicity, biopersistence, immunogenicity, genotoxicity…), it is also essential to understand the transformation of nano-objects in living environment in order to unravel the mechanisms determining their fate. In that regards, we report a valuable methodology to monitor nanoparticle biodegradability from macroscopic to nanometric levels. This multi-scale approach consist in following the magnetic and structural transformations of multicore maghemite nanoflowers in a medium mimicking intracellular lysosomal environment, where the nano-objects injected in vivo are usually confined. By confronting atomic-scale and macroscopic information on the biodegradation of these complex nanostuctures, we have determined the mechanisms involved in the critical alterations of their hyperthermic power and their Magnetic Resonance imaging T1 and T2 contrast effect. This complete annihilation of the technologically relevant properties of these nanoflowers highlights the harmful influence of cellular medium on the therapeutic and diagnosis effectiveness of iron oxide-based nanomaterials. To overcome this issue, we demonstrate that the coating of inert gold layer changes the surface reactivity of the nanosystems and protects the iron-oxide core from degradation. Such inorganic nanoshields could be a relevant strategy to modulate the degradability and ultimately the long term fate of nanomaterials in the organism. More generally, by examining the influence of the biological medium on the structure and physical properties of nano-objects, our material science approach opens up a new way to evaluate the life cycle of nanoparticles and their biodegradation products and provides relevant information on the design of safer and more efficient nanomaterials. Convinced that this article can be of broad interest for the readership of Small, we hope you will find this work attractive and look forward to hearing from you.

	Thank you for your attention to our contribution. With Kind Regards, Damien ALLOYEAU & Florence Gazeau (corresponding authors)
Corresponding Author Secondary Information:	
Corresponding Author's Institution:	Univerisité Paris Diderot
Corresponding Author's Secondary Institution:	
First Author:	Yasir Javed
First Author Secondary Information:	
Order of Authors:	Yasir Javed
	Lenaic Lartigue
	Pierre Hugounenq
	Quoc Lam Vuong
	Yves Gossuin
	Rana Bazzi
	Claire Wilhelm
	Christain Ricolleau
	Florence Gazeau
	Damien Alloyeau
Order of Authors Secondary Information:	
Abstract:	Understanding the relation between the structure and the reactivity of nanomaterials in the organism is a crucial step towards efficient and safe biomedical applications. The multi-scale approach reported here, allows following the magnetic and structural transformations of multicore maghemite nanoflowers in a medium mimicking intracellular lysosomal environment. By confronting atomic-scale and macroscopic information on the biodegradation of these complex nanostuctures, we can unravel the mechanisms involved in the critical alterations of their hyperthermic power and their Magnetic Resonance imaging T1 and T2 contrast effect. This transformation of multicore nanoparticles with outstanding magnetic properties into poorly magnetic single core clusters highlights the harmful influence of cellular medium on the therapeutic and diagnosis effectiveness of iron oxide-based nanomaterials. As biodegradation occurs through surface reactivity mechanism, we demonstrate that the inert activity of gold nanoshells can be exploited to protect iron oxide nanostructures. Such inorganic nanoshields could be a relevant strategy to modulate the degradability and ultimately the long term fate of nanomaterials in the organism.

Submitted to small NANO MICRO

Biodegradation mechanisms of iron oxide monocrystalline nanoflowers and tunable shield effect of gold coating

Yasir Javed,[1] Lénaic Lartigue,[1,2] Pierre Hugounenq,[3] Quoc Lam Vuong,[2,4] Yves Gossuin,[4] Rana Bazzi,[5] Claire Wilhelm,[2] Christian Ricolleau,[1] Florence Gazeau,[2] and Damien Alloyeau,[1*]*

[1] Laboratoire Matériaux et Phénomènes Quantiques, UMR 7162 CNRS/Université Paris Diderot, 10 rue Alice Domon et Léonie Duquet, F-75205 Paris Cedex 13, France.
[2] Laboratoire Matières et Systèmes Complexes, UMR 7057 CNRS/Université Paris - Diderot, 10 rue Alice Domon et Léonie Duquet, 75013 Paris, France
[3] Laboratoire Physico-Chimie des Electrolytes, Colloïdes et Chimie Analytique, UMR 7195 CNRS/Université Pierre et Marie Curie/ESPCI, 4 place Jussieu, F-75252 Paris Cedex 05, France.
[4] Service de Physique Biomédicale, Université de Mons, 20 Place du Parc, 7000 Mons, Belgium[5] Institut UTINAM, UMR 6213 CNRS/Université de Franche-Comté, 16 route de Gray, 25030 Besançon, France

[*] These authors contributed equally.
Corresponding authors: Dr. Damien ALLOYEAU, damien.alloyeau@univ-paris-diderot.fr,
Dr. Florence GAZEAU, florence.gazeau@univ-paris-diderot.fr

Supporting Information is available on the WWW under http://www.small-journal.com or from the author.

Keywords: Magnetic nanoparticles, degradation, iron oxide, magnetic resonance imaging, hyperthermia, gold

Abstract

Understanding the relation between the structure and the reactivity of nanomaterials in the organism is a crucial step towards efficient and safe biomedical applications. The multi-scale approach reported here, allows following the magnetic and structural transformations of multicore maghemite nanoflowers in a medium mimicking intracellular lysosomal environment. By confronting atomic-scale and macroscopic information on the biodegradation of these

complex nanostuctures, we can unravel the mechanisms involved in the critical alterations of their hyperthermic power and their Magnetic Resonance imaging T_1 and T_2 contrast effect. This transformation of multicore nanoparticles with outstanding magnetic properties into poorly magnetic single core clusters highlights the harmful influence of cellular medium on the therapeutic and diagnosis effectiveness of iron oxide-based nanomaterials. As biodegradation occurs through surface reactivity mechanism, we demonstrate that the inert activity of gold nanoshells can be exploited to protect iron oxide nanostructures. Such inorganic nanoshields could be a relevant strategy to modulate the degradability and ultimately the long term fate of nanomaterials in the organism.

1. Introduction

Given the growing use of nanomaterials in daily life products and their many promising applications in biomedicine, humans are expected to be increasingly exposed to nano-objects. Consequently, many research efforts are presently focused on the life cycle and toxicity of nano-sized materials.[1, 2] However, the emerging field of nanotoxicity must be considered from different angles. While most toxicology studies warn about the effects of nanomaterials on biological functions (cytotoxicity, biopersistence, immunogenicity, genotoxicity…), it is also essential to understand the transformation of nano-objects in living environment in order to unravel the mechanisms determining their fate.[3] By examining the influence of the biological medium on the structure and physical properties of nano-objects, the material science approach

opens up a new way to evaluate the life cycle of nanoparticles and their biodegradation products and provides relevant information on the design of safer and more efficient nanomaterials.

In addition to the nature of the materials and surface properties,[4, 5] the morphology and architecture of nanostructures are crucial determinants of their physical properties and outcome in the organism.[6] Multicore assembly of nanoparticles have been proposed for medical applications due to enhanced properties as contrast agent for imaging, nanoheaters for thermotherapy and mesoporous drug carrier for sustained drug delivery.[7-12] The capability of multicore structures to disintegrate into smaller entities might be a key advantage to penetrate tumor environment, reduce biopersistence and facilitate degradability and/or excretion.[13, 14] Therefore there is a crucial need in controlling the biodegradation of such structures by following their physical properties and morphological transformations. In spite of the tremendous potential of iron oxide nanoparticles (NPs) in the biomedical field, not enough attention has been paid to their biodegradation mechanisms. [15, 16][17-22] As most inorganic nanomaterials interacting with cells, iron oxide NPs are rapidly confined within intracellular lysosomes, where they are exposed to the combined effect of acidic pH around 4.7, digestive enzymes and iron chelators involved in iron regulation. Recently, we have evidenced that the biotransformation of iron oxide nanospheres and nanocubes takes place in this lysosomal environment, resulting in a transfer of iron from synthetic particles to ferritin proteins.[18, 23] However, although *in vivo* experiments are necessary to understand the pathway for biotransformation of inorganic NPs, the impossibility of analyzing the atomic structure and properties of the same NPs over time in living environment, prevents the understanding of the atomic-scale mechanisms leading to the degradation products. The methodology reported here gives the opportunity to follow both the magnetic and structural transformations of multicore maghemite nanoflowers (NFs) in a medium mimicking intracellular

lysosomal environment. The combined use of aberration-corrected high resolution transmission electron microscopy (HRTEM) and magnetic measurements allows confronting atomic-scale and macroscopic information on the biodegradation mechanisms of iron oxide NFs. Through this magneto-structural approach, we aim to establish the link between the structural degradation of the multicore NFs and the critical alterations of their hyperthermic power and their Magnetic Resonance Imaging T_1 and T_2 contrast effect. Therefore, we provide a deeper understanding of the harmful influence of cellular medium on the therapeutic and diagnosis effectiveness of complex iron oxide nanostructures. Finally, we suggest that the coating of a protective gold layer on maghemite, in addition to potentiate the efficiency of nanostructures for many biomedical applications, is an interesting strategy to slow-down the degradation kinetic of the iron oxide multicore structures.

2. Results

Iron oxide nanoflowers consist of an isotropic assembly of cores, forming nearly spherical porous supercrystals (**Figure 1**a). During the polyol synthesis of the nanoflowers, the merged cores rotate to share the same crystalline orientation and then minimize their surface energy.[24] Therefore, NFs exhibit a mono-crystalline inverse spinel FCC structure. Recently we have shown that the distinctive architecture of multicore iron oxide nanoparticles accounted for their outstanding efficacy as both heating mediators for magnetic hyperthermia and MRI contrast agent.[10] The magnetic properties of multicore particles have been compared to those of single cores, revealing a cooperative behavior due to exchange interactions between the cores constituting the particles. This collective magnetic behavior of internal cores was possible due to

the crystal continuity at the core interface, which also ensured a continuity of spin orientation. As a consequence, the multicore particles showed enhanced susceptibility compared to single core, while maintaining a superparamagnetic behavior due to a reduced surface anisotropy. The combination of their high susceptibility, high saturation magnetization and low magnetic anisotropy for particles of 24 nm size were responsible for their outstanding heating power and MRI relaxivities. Hence those biocompatible water-dispersed multicore particles, which are made of pure iron oxide, hold great promises for biomedical applications.

2.1 Time evolution of magnetic properties in the lysosome-like medium

The reactivity and degradation of multicore NFs were first monitored by measuring the evolution of their magnetic properties in a medium mimicking the lysosomal environment. A suspension of multicore NFs (10 mM iron concentration) was exposed to an acidic buffer at pH 4.7 supplemented with 20 mM citrate for a period of 23 days at 37°C. This simple medium containing citrate as iron chelators has been shown to efficiently trigger the degradation of single core iron oxide nanoparticles used as MRI contrast agent.[23, 25] This medium was first proposed by Arbab et al[26] to mimic lysosomal environment. The field-dependence of the magnetization was first probed at 310K by VSM measurements on the NF colloidal suspension. As observed in Figure 1b, the magnetization was reversible (no hysteresis) and was rapidly saturating when increasing the magnetic field beyond 200 kA/m, regardless of the incubation time in the lysosome-like buffer. However, in the meantime, the saturation magnetization of the suspension exponentially decreased, losing 83% of its initial value after 23 days in the acidic buffer (Figure 1b, **Table 1**). This loss of magnetization could be explained by the complete dissolution of some nanoparticles in the acidic medium and/or by their transformation into less magnetic structures. A

closer view into the low field magnetization (Figure 1c) shows that the initial susceptibility is also diminished over time in the acidic medium. This suggests that the particles are being transformed and potentially break down their multicore structure. Indeed the distribution of the "effective" magnetic size of the particles can be deduced from a fit of their magnetization curve by a Langevin function weighted by the magnetic size distribution[25] (see Table 1 and **Figure S1 in Supplementary Materials**). The initial multicore nanoparticles show a broad log-normal distribution of their magnetic sizes centered around 14 nm (Figure 1d). As discussed in our previous work,[10] this effective magnetic size is larger than the TEM size of each constitutive core (10.6 nm). Consistently the saturation magnetization M_S of NFs is 82 $A.m^2.kg^{-1}$ (close to the bulk value of maghemite) while it is reduced to 58 $A.m^2.kg^{-1}$ for 10.6 nm single cores.[10] Upon exposure to the acidic citrate buffer, the magnetic size of particles tends to diminish and after three weeks, the distribution becomes narrow around a mean diameter of 12.2 nm, suggesting the loss of their multicore organization. In line with macroscopic magnetization measurements, electron microscopy confirms the physical transformation of NFs (**Figure 2**): the multicore initial structures (with a mean TEM diameter of 24 nm) seem to dissociate into smaller single cores over time. At day 23, some degraded structures clearly coexist with some single cores, resulting in a bimodal distribution of TEM size. After three months, the scarce resilient particles all appear as single core with a mean size of 8-10 nm (Figure 2).

Ferromagnetic resonance (FMR) spectroscopy also provides a nanometrology method to investigate the spin dynamics in nanoparticles and its evolution in the acidic medium. Initial multicore particles show a complex asymmetric resonance spectrum at 9.25 GHz comprising several absorption lines, whereas single cores of 10.6 nm exhibit a single symmetric resonance centered on 3 kOe. The asymmetry of the resonance spectrum of the multicores can be ascribed

to the exchange interactions at the core boundary, while the broad spectrum of single core is attributed to a large surface anisotropy.[10, 27] Here we observe that, upon degradation in the lysosome-like, FMR spectra evolve from the asymmetric shape characteristic of the multicores to the symmetric shape of the single core (Figure 1e). In addition the area of the absorption spectrum (FMR absorption signal), which is a measure of the ferrimagnetic materials in the suspension,[25] rapidly decreases over time in acidic buffer (Figure 1f) in line with the decrease of saturation magnetization. This supports the hypothesis that NFs are degraded into single cores, while an increasing mass of iron is released from ferromagnetic lattice and forms non-magnetic chelates with citrate. It is worthy to note that the transition from asymmetric to symmetric FMR line occurs from day 3 to day 5, suggesting that exchange interactions at the core boundaries might be early affected. Because some multicore structures are still observed on TEM at time points up to three weeks, we hypothesize that magnetic hallmarks of NFs are debased in acidic medium before the complete degradation of multicore organization as observed by TEM.

The next step was to investigate how such structural and magnetic transformations of NFs might affect their efficiency for therapeutic and imaging applications. The specific absorption rate (SAR) of nanoparticles was measured in an alternating magnetic field of 24 $kA.m^{-1}$ at a frequency of 520 kHz. The SAR, determining the heating power of nanoparticles, is governed by key parameters of nanoparticles which comprise their magnetic anisotropy, size, susceptibility and saturation magnetization.[28, 29] Recently, we have shown that the nanostructuration of single-core to multi-core structure increases the SAR from 150 W/g to 1604 W/g.[10] Here the exposure to acidic medium has a dramatic effect on the SAR. After 6 days, the heating power decreases by 70%, from 1761 W/g to 552 W/g, and fall to no more than 19 W/g after 23 days (**Figure 3**a, Table 1). This effect testifies not only the early loss of magnetic hallmarks due to multicore

nanostructuration but also undeniably reflects the dissolution of nanoparticles. Altogether it highlights the potential deterioration of heating efficiency of multicore nanoparticles that are uptaken by cells (including cancer cells) and underwent lysosome degradation.

Finally we focused on the contrast properties of NFs for magnetic resonance imaging. The use of superparamagnetic nanoparticles as MRI contrast agent relies on the accelerated relaxation of the magnetization of water protons diffusing in local magnetic fields created by particles. The spin-lattice (r_1) and spin-spin (r_2) relaxivities are defined as the increase of the longitudinal and transverse relaxation rate of the medium (here water or acidic buffer) induced by 1mM of the magnetic agent (here iron). The improvement of sensitivity in MR sensing and imaging requires an optimization of both r1 and r2 in the application medium. As magnetic nanoparticles are readily internalized by cells *in vitro* and particularly by macrophages *in vivo*, the persistence of their contrast properties within intracellular lysosomes is an important concern for the success of long term cell tracking by MRI. However little is known on the outcomes of nanoparticle degradation in lysosomes,[26] partly because a number of environmental factors, including nanoparticles distribution, aggregation, magnetic interactions and lysosomal confinement,[30, 31] actually change the relaxivities of intracellular nanoparticles. NFs possess very large r_1 and r_2 relaxivities that surpass that of single core particles and may be attributed to their multicore structure.[10] More particularly the nuclear magnetic resonance dispersion (NMRD) profile, which provides r_1 measurements over a wide range of ^{1}H resonance frequency (0.015 MHz to 40 MHz) or equivalently of the magnetic field strength (0.35 mT to 0.94 T) demonstrates for NFs a monotonous decrease of r_1 relaxivity with increasing frequency and exceptionally high relaxivity value at low fields. Such behavior is unusual for superparamagnetic particles which generally show a maximum of r1 at a field which depends on the dynamics of the particle magnetic

moment.[32] However Lévy et al established that the low field longitudinal relaxivity could be considerably enhanced and could make disappear the typical r_1 maximum when the fluctuations of the transverse component of the particle magnetic moment are slowed down.[33] As NFs are in the limit of the superparamagnetic regime, this model could account for their exceptionally high relaxivity at low fields. In the present study, we measured the NMRD profile of NFs at different time-points in the lysosome-like medium. As expected from the loss of nanoparticles magnetization reported above, the longitudinal relaxivity dramatically diminished at long time in the acidic medium regardless of the ^{1}H resonance frequency (Figure 3b). However, at short times, we first observed a 25% decrease of the r_1 relaxivity as soon as NFs are transferred from water to acidic medium (0 day) which accentuates to 73% after one day and then retrieve 45% of its initial value in water at day 3 and continuously decreases at longer time-points. The transverse relaxivity r_2 measured at 20 MHz exhibits a similar variation over time in lysosome-like medium (Figure 3d). To understand this non-monotonous temporal variation of relaxivities, we recall the importance of nanoparticle aggregation on their relaxation properties. Indeed very large clusters of particles cannot be detected by NMRD profile: their corresponding r_1 is too small at the used magnetic fields.[34] Agglomeration of nanoparticles above a critical volume also diminishes the transverse relaxation rate r_2.[35, 36] Here, nanoflowers might be more prone to aggregation than single cores due to their large diameter and enhanced magnetic interactions. We thus investigated the colloidal stability of NFs by magnetically-induced birefringence measurements, a previously described method that probe the orientational dynamics of magnetic particles in response to a magnetic field.[37] Interestingly the mean hydrodynamic diameter of NFs was more than doubled in acidic medium in comparison to the initial water suspension (91.5 nm versus 37 nm) and further increased after one day (101.4 nm), indicating the formation of small aggregates of

citrate-coated NFs at pH 4.7 (Table 1 and Figure 3e). Beside such small aggregates that remain dispersed in the suspension, we also observed some large sedimenting agglomerates that were not probed by the birefringence experiment. Nevertheless from day 2 in acidic medium, the whole suspension becomes limpid and the hydrodynamic diameter starts to decrease and fall down to 18 nm, below the initial value in water. This suggests that the degradation of magnetic properties and of multicore organization reduces the propensity of particles to form aggregates or chains and that the degrading particles become isolated while diminishing in size (Figure 2). In line with these results, the temporal evolution of relaxivities results from the interplay between the aggregation effect until day 2, the disaggregation effect at intermediate time (which increases r_1) and the progressive loss of magnetic materials (which further decreases r_1 and $r_{2)}$. To test this hypothesis, we changed the anionic monomeric citrate coating of NFs for a polymeric anionic coating made of poly(acrylic) acid (PAA). PAA-coated NFs have a larger hydrodynamic size in water (70 nm) compared to citrate-coated NFs, but are less aggregated in the acidic medium due to steric hindrance and reduced dipole-dipole interactions (**Supplementary Figure S2**). Consistently their hydrodynamic diameter slowly diminishes in the acidic buffer and the r_1 relaxivity progressively decreases with time mainly due to the loss of magnetic properties. In contrast to the relaxivity measurements which are very sensitive to the local arrangement of particles,[36] the type of coating –PAA versus citrate – has a marginal effect on the loss of nanoparticle magnetization and FMR absorption which reflect similar diminution of magnetic materials. Hence while the transient aggregation of citrate-coated NFs strongly impact relaxivites at short times, the gradual deterioration of magnetic properties and multicore structure plays in concert to diminish r_1 and r_2 at longer time. Interestingly, the shape of the NMRD profile at the longest time investigated (14 days) was shifted to higher magnetic field in comparison to the

initial shape, showing a shoulder that is characteristic of smaller single core particles, suggesting the loss of cooperative magnetic behavior (Figure 3c). This interpretation can be quantitatively confirmed by fitting the NMRD profiles. The usual equations for relaxation induced by superparamagnetic nanoparticles[32] were used and the corresponding NMR sizes extracted. These sizes correspond to the minimal approach distance between the water molecules and the magnetic particles – as a consequence, they are larger than the magnetic core size but smaller than their hydrodynamic size, which is verified in our case (see Table 1). As NFs are in the limit between the low and high anisotropy energy limit, the obtained parameters must be carefully interpreted. The *rigid dipole model* of Levy et al[33] was also used for comparison and correctly fit the data with similar NMR sizes. During the first 6 days, some NFs (with a slightly smaller size than the initial one) remain in the solution while large aggregates cannot be detected by NMRD profiles. At day 14, the obtained NMR size is twice smaller, which is consistent with the fact that a large amount of NFs is degraded into smaller isolated single cores.

In conclusion, we have shown that monitoring the macroscopic properties of an assembly of multicore nanoparticles, such as their magnetic and FMR properties, heating power or MR relaxivity, provides an accurate methodology to follow their degradability and to predict their behavior in a simple model of intracellular environment. It is worth noticing that both magnetic and structural properties of the NF remain unaltered over several months into water **(see supporting information, Figure S3)**. In what follows, we focus on the evolution of single particles at the nanoscale in order to highlight the mechanisms of degradation.

2.2 Atomic-scale investigations of the degradation mechanisms

The nanoparticle degradation was characterized at the atomic level using aberration-corrected HRTEM on NFs flatly deposited on a lacey carbon-coated TEM grid. The grid was immersed into the acidic buffer for different time periods, and the nanoparticle evolution was probed after each immersion step. First, about 100 isolated NFs were localized on the grid and identified to monitor their degradation kinetic. This statistical analysis summarized in **Figure 4**a reveals the high reactivity of NFs structures in the lysosome-like medium. Indeed, the atomic structure of all the isolated particles is damaged after only 30 minutes of immersion. However, although the NFs promptly show signs of structural degradation, these latter do not systematically induce the complete dissolution of NFs. The percentage of totally dissolved NPs increases from 5 % after 30 minutes to 45 % after 100 minutes and stays below 50% after 140 minutes. This asymptotic behavior is consistent with the many single core nanoparticles observed in the lysosome-like medium after several weeks of immersion (Figure 2) and indicates that these single core structures are much more stable in the medium than the multi-core architecture of the initial NFs. As previously observed on nanocubes,[23] the degradation is faster on two dimensional grid in comparison to the suspension probably due to a larger ratio of available citrate chelators per particle. In addition the spatial organization of iron oxide NPs has also a strong influence on their reactivity to the lysosome-like medium.[23] While the acidic medium always causes severe damages to the structure of isolated NFs, the aggregation of NFs significantly slows down their degradation kinetic (**see supporting information, Figure S4**). The reinforced stability of large three-dimensional assemblies may relate to the reduced accessibility of iron oxide surface for the chelating agents. Thus agglomeration tendency of nanoflowers, which occur following internalization into early endosomes and lysosomes,[10] could severely diminish their reactivity and short time degradation kinetics in the organism.

Following at high resolution the degradation of individual NFs sheds light on the atomic process involved in the transformation of multicore nanoparticles with promising magnetic properties into poorly magnetic single core. As observed in Figure 4b-c, the gradual corrosion of the NP surface results in a clear size decrease of the NFs, but the initial atomic arrangement of nanoparticles is maintained throughout the degradation process. This result confirms that the alteration of the NF atomic-structure in intracellular-like environment is controlled by surface reactivity mechanisms. Simultaneously, we observe the formation of holes into the atomic structure of the NFs which appears as brighter contrast on TEM images. The atomic-scale study of this milling process shows that these holes are formed on structural defaults of the initial NFs (Figure 4c). Indeed, the multicore architecture of the NFs gives rise to porous atomic surfaces. These pores are more vulnerable to chelating agents either because of the change in coordination number due to surface curvature and defects, or because of a possible lack of protecting coating inside these nano-cavities. Consequently, the degradation kinetic is faster inside the pores and their size increases from 1 to 20 nm^2 within the first minutes of immersion. Surprisingly, the structure of the resulting holes reveals that the corrosion mechanisms are also influenced by the thermodynamic properties of the iron oxide structure. Indeed, when the degraded NFs are oriented along the [001] zone axis the enlarged pores consist in rectangular patterns sharing the same orientation. By comparing the structural information from the direct and Fourier spaces, we observe that the rectangular holes are oriented along the [400] and [040] directions. The formation of these {400}-type facets suggests that these particular surfaces are less reactive (i.e. more stable in the buffer medium) and consequently the degradation kinetic is slower along the [400]-type directions. This result is consistent with the degradation of iron oxide nanocubes,[23] which preferentially occurs on small {220} facets than on large {400} facets. Nevertheless, this higher

stability remains insufficient to avoid the step by step degradation of iron oxide NFs. The gradual corrosion of the iron oxide surfaces, which is enhanced though the pores of the NFs structure, inevitably induces a size reduction of the multicore particles and leads to the separation of the single cores. This mechanism is consistent with the long term TEM observation described in Figure 2 showing that single core NPs are mainly found in the lysosome-like solution after three weeks of immersion.

2.3 Slowing-down the degradation kinetic with a gold-protective layer

Among many parameters influencing the fate of NPs inside cells (size, shape, composition…), the key role of nanoparticle functionalization has been reported. [23][38] By raising the first barrier against environmental reagent, the nature and distribution of organic/inorganic coating might be a crucial determinant of the degradability of nanoparticles. Here, we investigate the influence of gold inorganic coating on the corrosion of iron oxide NP in lysosome-like media. Gold layers with nominal thicknesses of 3, 5 and 7 nm were physically deposited by pulsed laser deposition over NF samples. Bragg filtered high resolution imaging was used to generate chemical maps exhibiting the distribution of both Au and iron oxide within the nanostructures and then analyze the morphology of the gold layers depending on its nominal thickness. The isolated gold clusters observed on the NFs with the thinnest protective layer (**Figure 5**a, nominal thickness of 3 nm) reveals the poor wetting properties of gold over iron oxide. To minimize its interface energy the gold layer tends to reduce its cover rate by forming isolated 3D islands over the NFs. By increasing the quantity of Au, this Volmer-Weber growth mode leads to a percolated film over the magnetic NPs (Figure 5b, nominal thickness of 5 nm). Finally, NFs coated with a continuous

granular Au layer were obtained with a nominal thickness of 7 nm (Figure 5c). The true thickness of this full metal layer is 3 nm.

These three types of core-shell nanostructures were then immersed into the buffer medium for different time periods, and the nanoparticle evolution was probed after each immersion step by using both Bragg filtered high resolution TEM and energy dispersive X-ray (EDX) nano-analysis. By combining the imaging and analytical capabilities of TEM we can quantitatively characterized the degradation of the magnetic cores as a function of the incubation time, by following their size reduction and the evolution of the Fe/Au composition ratio within individually-analyzed core-shell NPs. Chemical imaging of the magnetic cores before incubation and after 45 minutes in the lysosome-like medium illustrates that isolated Au clusters and percolated Au films cannot prevent the fast size-reduction of the iron oxide NFs (**Figures 6**a and 6b). On the contrary, continuous Au shells seem to be an efficient shield layer against surface corrosion, since the size of the fully-covered magnetic cores remains almost constant in the acidic medium (Figure 6c). EDX nano-analyses reinforce this conclusion, given that the Fe/Au composition ratio within single core-shell NPs remains constant when the gold layer is continuous, where as it decrease by 25% and 70 % over one hour, for gold layers consisting in percolated film and isolated clusters, respectively (Figure 6d). These nano-scale analyses reveal that the kinetic of degradation of the iron oxide NFs clearly depends on the cover rate of the Au layer: the lower the cover rate, the better the accessibility for the chelating agent and consequently the faster the corrosion of the magnetic cores. It is worth noticing that there is currently great interest in the development of such NPs composed of magnetic cores with plasmonic shell layers that combines magnetic and plasmonic properties for theranostic applications. [39-41] In that regard, gold layers are promising candidates because of their shape-dependent plasmonic properties and their biocompatibility.

Here, we shed light on the protective properties of gold layers that could also be exploited to avoid a too fast annihilation of the magnetic properties of iron-oxide nano-objects due to the deterioration of their atomic-structure in cell compartments. This potential application of gold nano-shields arises from their very low biodegradability, as gold is mostly inert to chemicals it should encounter inside the body.[42] It is interesting to note that the thickness and morphology of the gold coating (here obtained by physical deposition) could be modulated in order to tune the degradation rate of NFs. Whenever this gold shield strategy could be achieved with colloidal chemical synthesis of core-shell nanocomposites, [43, 44][45][46] it would give the unique opportunity to control the degradability of NFs so that they keep their magnetic properties for the time of therapeutic treatment and degrade at longer time to be locally processed by iron metabolism or eliminated by biliary excretion. This concept of hybrid nanostructures with materials possessing different reactivity to their environment opens new route for the modulation of nanoparticle fate in the organism. Further studies are necessary to assess this strategy *in vivo*.

3. Conclusions

In conclusion, we have presented a valuable methodology to monitor nanoparticle biodegradability from macroscopic to nanometric levels. We manage to correlate the atomic scale transformations of multicore monocrystalline nanostructures to the evolution of their magnetic properties over time in lysosome-like medium. The remarkable cooperative behavior of the iron oxide nanoflowers is progressively impaired in lysosomal acidic medium due to the porous widening and dissociation of single cores. Hence intracellular uptake should rapidly jeopardize the NF's outstanding properties for magnetic hyperthermia and MRI detection, while it enables dissociation and further dissolution of nanocrystals. The balance between crystal corrosion,

release of iron species and local processing of iron by iron storage protein should be finely regulated in order to avoid toxic effect due to Fenton reaction. Hence it should be advantageous for both therapeutic efficiency and safety issue to control the intracellular degradation rate of nanostructures. In that regards, we demonstrate that the organization of iron oxide NPs has a significant impact on their reactivity in lysosome-like medium, since aggregation provides protection against degradation, while separation encourages the transformation processes. We also suggest a strategy using gold nanoshield at the surface of the particles to modulate their degradability and ultimately their long term fate in the organism.

4. Experimental Section

Nanoflower synthesis: magnetite NFs were synthesized following the procedure described in Hugounenq et al[24] which uses alkaline hydrolysis of FeCl3·6H2O and FeCl2·4H2O with stoichiometric ratio in a mixture of polyols (diethylene glycol (DEG) and Nmethyldiethanolamine (NMDEA), 1:1 w/w) at 220 °C.

The choice of the solvents, the nature of the precursors, progressive heating to 220°C (2 °C per min) and constant stirring at 220°C for 12 hours were critical factors to obtain multicore monocrystalline nanostructures with monodisperse size. A 8M solution of iron nitrate was added to the particles and heated at 80 °C for 45 min to achieve a complete oxidation of the magnetite nanoparticles into maghemite. After another treatment with 10% nitric acid, the particles were washed and redispersed in water. At this stage, the aqueous dispersion of NFs was stable in acid or basic conditions with a point of zero charge near pH 7.3. Citrate anions were grafted to NF surface by adding 0.3 mol of sodium citrate per 1 mol of iron element in order to ensure colloidal

stability at physiological pH. Alternatively, NFs were coated with polymeric poly(acrylic) acid (PAA) by ligand exchange. To achieve a stable coating, a large excess of PAA molecules were added to the nanoparticles suspension in acidic conditions (pH 2). At this pH the PAA molecules are weakly charged and the nanoparticles can be washed using magnetic decantation to remove the excess of PAA. The nanoparticles are then redispersed by increasing the pH to 9 by adding a concentrated solution of NH_4OH. The nanoparticles suspension is then dialyzed in water using a 12kDa membrane to remove the remaining free PAA molecules.

Magnetic measurements: Magnetization measurements were carried out on a with a Quantum Design MPMS-5S SQUID magnetometer. All magnetic measurements were performed in solutions around 10 mM in iron and the data were corrected from the diamagnetic contribution of water and sample holder. The field-dependent magnetization curve was measured at 310K in the range between 0 and 3 Tesla. The distribution of apparent magnetic size was obtained from the fit of magnetization curve using a Langevin function weighted by a log-normal distribution of magnetic diameter (characteristic diameter d_{mag}, polydispersity index σ) as previously described.[25]

Ferromagnetic resonance (FMR) spectra were obtained using a Varian ESR spectrometer operating at 9.26 GHz (X band) with following parameters: microwave power = 1 mW, modulation frequency = 100 kHz, modulation field = 10 Gauss. FMR spectra were recorded at room temperature for 2 μL of NF suspension at iron concentration of 10 mM. Quantification of the remaining magnetic iron in the suspension was obtained by double integration of the FMR spectrum and comparison to a calibration curve of non-degraded NFs. It was verified that paramagnetic iron species that could be released in the medium were not contributed to the FMR signal at room temperature.

Hyperthermia Measurement. The evaluation of heat generation was performed with a home-built magnetothermal setup[28] consisting of a resonant RLC circuit with a 16 mm coil. The field amplitude was fixed to 24 kA/m and the frequency to 520 kHz. 300 μL of the NF solution was put inside the thermalized coil and the temperature was probed with a fluoro-optic fiber thermometer (Luxtron Corp., CA) every 0.7 s.

The SLP was calculated using the following formula:

$SAR = \frac{1}{m_e}\left(\sum_i c_i m_i \frac{dT}{dt}\right)$ where m_e is the total mass of the iron, c_i is the specific heat, and m_i is the weight of the different species in solution (particles and water) and dT/dt is the slope of the initial temperature increase. The mass of iron was measured by flame atomic absorption spectroscopy.

NMRD experiments: The frequency dependence of the ^{1}H longitudinal relaxation time 1/T1 in NF aqueous suspensions was recorded over the frequenc range of 0.015 to 40 MHz using a Spinmaster FFC-2000 fast-field cycling NMR relaxometer (Stelar SRL, Mede, Italy).

The temperature of the samples was maintained at 37°C using a thermostated airflow system. All of the ^{1}H magnetization recovery curves were singly exponential within experimental error, and the random errors in fitting T_1 were always less than 1%. T_2 was measured using the CPMG pulse sequence on a 20MHz Bruker minispec. The relaxivity r_i was obtained by normalizing the relaxation rate ($1/T_i$ - $1/T_{water}$) with the iron concentration of the sample determined by Inductively coupled plasma mass spectroscopy.

Magnetically-induced birefringence experiment: The change in hydrodynamic diameter caused by the onset of aggregation was determined by means of a magnetically-induced birefringence experiment which is described in detail elsewhere.[47] Briefly, in the presence of an external

magnetic field, the NF suspension acquires a birefringence Δn ($\Delta n = n_{\parallel} - n_{\perp}$, $n_{\parallel}$ and $n_{\perp}$ being the optical indexes, respectively, in the direction of the magnetic field and perpendicular to it), due to the alignment of optical axes of the nanoparticles along the field and the subsequent alignment of their optical anisotropy axes. This birefringence induces a phase lag φ proportional to Δn, which is measured through a polarizer and analyser. The NF suspension sample is submitted to a pulsed vertical magnetic field (100 Oe) and the transmitted light *I(t)* is collected on the photodetector (PD). The birefringence decay is averaged over a large number of pulses (typically 512, total time of measurement 20s) and analysed using a stretched exponential. The distribution of hydrodynamic diameter is deduced from stretched exponential parameters as previously described. [37]

Aberration-corrected HRTEM: TEM investigations were performed with the JEOL ARM 200F microscope operating at 200 kV. This microscope is equipped together with a CEOS aberration corrector and a cold field emission gun.[48, 49] Lacey carbon TEM grids (agar) were used to follow the degradation mechanisms by HRTEM. The recognizable patterns of the lacey carbon film facilitate the step-by-step following of the nanostructure alteration. Bragg filtered high resolution imaging is a method of choice to study the structure of non-miscible nanohybrides. This post-acquisition image processing consist in calculating the inverse Fourier transform of the power spectrum of an HRTEM image, on which a well defined spatial frequency is selected with a low-pass filter. This technique is also called digital dark field imaging since the low pass filter plays the same role as the objective aperture in conventional dark field imaging.[50, 51] By selecting suitable reflections for the crystal lattice of gold or iron oxyde, one obtains a chemical mapping exhibiting the distribution of the two species in the nanoparticles. One displays in fact the part of the nanocrystal where distances between interference fringes (i.e. atomic planes)

correspond to the selected reflections on the power spectrum. We note that such a chemical imaging required a clear visibility of the atomic structure on the whole studied nanocrystal. In that regard, we greatly benefit from sub-angstrom resolution imaging that allows observing the atomic structures of both gold and iron oxide almost independently their orientation.

Deposition of the gold protective layers*:* The gold layers were produced over the iron oxide NFs by pulsed laser deposition in a high vacuum chamber at room temperature.[52, 53] The pressure in the chamber is greater than 10^{-8} Torr. A typical target – substrate configuration was used to deposit Au by PLD using a KrF excimer laser working at a wavelength of 248nm with pulse duration of 25 ns at a repetition rate of 5Hz.The laser energy was 250mJ. The deposition rate of Au vapor phase was controlled by an *in situ* quartz crystal monitor, which indicates the nominal thickness of deposited materials on the quartz surface, in a continuous thin film approximation. Gold layers with nominal thicknesses of 3, 5 and 7 nm were prepared. As the iron-oxide nanoparticles are obviously not a smooth substrate, the nominal thickness of the deposited gold does not correspond to the true thickness of the gold layer.

Acknowledgements

This work was supported by the Region Ile-de-France (convention SESAME E1845 for the JEOL ARM 200F electron microscope installed at the Paris Diderot University), the ANR project Nanothermotherapy, the CNRS (Defi Nano project), the City Hall of Paris (*Research In Paris* Program), the F.R.S-FNRS, the Labex SEAM and the Higher Education Commission (HEC) of Pakistan (overseas scholarship scheme for MS/MPhil leading to Phd in selected fields phase-II, France). We are also grateful to François Gendron and to the MPBT Plateform for FMR and magnetic measurements.

References

[1] G. V. Lowry, K. B. Gregory, S. C. Apte, and J. R. Lead, *Environmental Science & Technology* **2012,** *46*, 6893.
[2] C. R. Thomas, S. George, A. M. Horst, Z. Ji, R. J. Miller, J. R. Peralta-Videa, T. Xia, S. Pokhrel, L. Mädler, J. L. Gardea-Torresdey, P. A. Holden, A. A. Keller, H. S. Lenihan, A. E. Nel, and J. I. Zink, *ACS Nano* **2011,** *5*, 13.
[3] C. Levard, E. M. Hotze, G. V. Lowry, and G. E. Brown, *Environmental Science & Technology* **2012,** *46*, 6900.
[4] T. Xia, Y. Zhao, T. Sager, S. George, S. Pokhrel, N. Li, D. Schoenfeld, H. Meng, S. Lin, X. Wang, M. Wang, Z. Ji, J. I. Zink, L. Mädler, V. Castranova, S. Lin, and A. E. Nel, *ACS Nano* **2011,** *5*, 1223.
[5] S. George, S. Lin, Z. Ji, C. R. Thomas, L. Li, M. Mecklenburg, H. Meng, X. Wang, H. Zhang, T. Xia, J. N. Hohman, S. Lin, J. I. Zink, P. S. Weiss, and A. E. Nel, *ACS Nano* **2012,** *6*, 3745.
[6] L. Guo, I. Panderi, D. D. Yan, K. Szulak, Y. Li, Y.-T. Chen, H. Ma, D. B. Niesen, N. Seeram, A. Ahmed, B. Yan, D. Pantazatos, and W. Lu, *ACS Nano* **2013,** *7*, 8780.
[7] T.-J. Yoon, H. Lee, H. Shao, S. A. Hilderbrand, and R. Weissleder, *Advanced Materials* **2011,** *23*, 4793.
[8] J. E. Lee, N. Lee, T. Kim, J. Kim, and T. Hyeon, *Accounts of Chemical Research* **2011,** *44*, 893.
[9] B. Luo, S. Xu, A. Luo, W.-R. Wang, S.-L. Wang, J. Guo, Y. Lin, D.-Y. Zhao, and C.-C. Wang, *ACS Nano* **2011,** *5*, 1428.
[10] L. Lartigue, P. Hugounenq, D. Alloyeau, S. P. Clarke, M. Lévy, J.-C. Bacri, R. Bazzi, D. F. Brougham, C. Wilhelm, and F. Gazeau, *ACS Nano* **2012,** *6*, 10935.
[11] C. Paquet, H. W. de Haan, D. M. Leek, H.-Y. Lin, B. Xiang, G. Tian, A. Kell, and B. Simard, *ACS Nano* **2011,** *5*, 3104.
[12] C. Cheng, F. Xu, and H. Gu, *New Journal of Chemistry* **2011,** *35*, 1072.
[13] C. Wong, T. Stylianopoulos, J. Cui, J. Martin, V. P. Chauhan, W. Jiang, Z. Popović, R. K. Jain, M. G. Bawendi, and D. Fukumura, *Proceedings of the National Academy of Sciences* **2011,** *108*, 2426.
[14] J. T. Jenkins, D. L. Halaney, K. V. Sokolov, L. L. Ma, H. J. Shipley, S. Mahajan, C. L. Louden, R. Asmis, T. E. Milner, K. P. Johnston, and M. D. Feldman, *Nanomedicine : nanotechnology, biology, and medicine* **2013,** *9*, 356.
[15] S. Kittler, C. Greulich, J. Diendorf, M. KÃ¶ller, and M. Epple, *Chemistry of Materials* **2010,** *22*, 4548.
[16] M. Chanana, P. Rivera_Gil, M. A. Correa-Duarte, L. M. Liz-Marzán, and W. J. Parak, *Angewandte Chemie International Edition* **2013,** *52*, 4179.
[17] R. Mejías, L. Gutiérrez, G. Salas, S. Pérez-Yagüe, T. M. Zotes, F. J. Lázaro, M. P. Morales, and D. F. Barber, *Journal of Controlled Release* **2013,** *171*, 225.
[18] M. Levy, N. Luciani, D. Alloyeau, D. Elgrabli, V. Deveaux, C. Pechoux, S. Chat, G. Wang, N. Vats, F. Gendron, C. Factor, S. Lotersztajn, A. Luciani, C. Wilhelm, and F. Gazeau, *Biomaterials* **2011,** *32*, 3988.
[19] R. Weissleder, D. D. Stark, B. L. Engelstad, B. R. Bacon, C. C. Compton, D. L. White, P. Jacobs, and J. Lewis, *AJR Am J Roentgenol* **1989,** *152*, 167.

[20] E. Okon, D. Pouliquen, P. Okon, Z. V. Kovaleva, T. P. Stepanova, S. G. Lavit, B. N. Kudryavtsev, and P. Jallet, *Lab Invest* **1994,** *71,* 895.
[21] K. Briley-Saebo, A. Bjornerud, D. Grant, H. Ahlstrom, T. Berg, and G. M. Kindberg, *Cell Tissue Res* **2004,** *316,* 315.
[22] H. Bernd, E. De Kerviler, S. Gaillard, and B. Bonnemain, *Invest Radiol* **2009,** *44,* 336.
[23] L. Lartigue, D. Alloyeau, J. Kolosnjaj-Tabi, Y. Javed, P. Guardia, A. Riedinger, C. Péchoux, T. Pellegrino, C. Wilhelm, and F. Gazeau, *ACS Nano* **2013,** *7,* 3939.
[24] P. Hugounenq, M. Levy, D. Alloyeau, L. Lartigue, E. Dubois, V. Cabuil, C. Ricolleau, S. Roux, C. Wilhelm, F. Gazeau, and R. Bazzi, *The Journal of Physical Chemistry C* **2012,** *116,* 15702.
[25] M. Levy, F. Lagarde, V. A. Maraloiu, M. G. Blanchin, F. Gendron, C. Wilhelm, and F. Gazeau, *Nanotechnology* **2010,** *21,* 395103.
[26] A. S. Arbab, L. B. Wilson, P. Ashari, E. K. Jordan, B. K. Lewis, and J. A. Frank, *NMR Biomed* **2005,** *18,* 383.
[27] F. Gazeau, J.-C. Bacri, F. Gendron, R. Perzynski, Y. L. Raikher, V. I. Stepanov, and E. Dubois, *Journal of Magnetism and Magnetic Materials* **1998,** *186,* 175.
[28] J. P. Fortin, C. Wilhelm, J. Servais, C. Menager, J. C. Bacri, and F. Gazeau, *J Am Chem Soc* **2007,** *129,* 2628.
[29] J. Carrey, B. Mehdaoui, and M. Respaud, *J Appl Phys* **2011,** *109,* 083921.
[30] M. Levy, F. Gazeau, J. C. Bacri, C. Wilhelm, and M. Devaud, *Phys Rev B* **2011,** *84,* 075480.
[31] M. Lévy, C. Wilhelm, M. Devaud, P. Levitz, and F. Gazeau, *Contrast Media & Molecular Imaging* **2012,** *7,* 373.
[32] S. Laurent, D. Forge, M. Port, A. Roch, C. Robic, L. Vander Elst, and R. N. Muller, *Chem Rev* **2008,** *108,* 2064.
[33] M. Lévy, F. Gazeau, C. Wilhelm, S. Neveu, M. Devaud, and P. Levitz, *The Journal of Physical Chemistry C* **2013,** *117,* 15369.
[34] Q. L. Vuong, Y. Gossuin, P. Gillis, and S. Delangre, *The Journal of Chemical Physics* **2012,** *137*.
[35] Q. L. Vuong, P. Gillis, and Y. Gossuin, *Journal of Magnetic Resonance* **2011,** *212,* 139.
[36] Q. L. Vuong, J.-F. Berret, J. Fresnais, Y. Gossuin, and O. Sandre, *Advanced Healthcare Materials* **2012,** *1,* 509.
[37] L. Lartigue, C. Wilhelm, J. Servais, C. Factor, A. Dencausse, J.-C. Bacri, N. Luciani, and F. Gazeau, *ACS Nano* **2012,** *6,* 2665.
[38] X. R. Xia, N. A. Monteiro-Riviere, S. Mathur, X. Song, L. Xiao, S. J. Oldenberg, B. Fadeel, and J. E. Riviere, *ACS Nano* **2011,** *5,* 9074.
[39] W. Brullot, V. K. Valev, and T. Verbiest, *Nanomedicine: Nanotechnology, Biology and Medicine* **2012,** *8,* 559.
[40] C. S. Levin, C. Hofmann, T. A. Ali, A. T. Kelly, E. Morosan, P. Nordlander, K. H. Whitmire, and N. J. Halas, *ACS Nano* **2009,** *3,* 1379.
[41] P. Quaresma, I. Osorio, G. Doria, P. A. Carvalho, A. Pereira, J. Langer, J. P. Araujo, I. Pastoriza-Santos, L. M. Liz-Marzan, R. Franco, P. V. Baptista, and E. Pereira, *RSC Advances* **2013,** *4,* 3659.
[42] N. Khlebtsov, and L. Dykman, *Chemical Society Reviews* **2011,** *40,* 1647.
[43] Z. Xu, Y. Hou, and S. Sun, *Journal of the American Chemical Society* **2007,** *129,* 8698.

[44] H. Yu, M. Chen, P. M. Rice, S. X. Wang, R. L. White, and S. Sun, *Nano Letters* **2005,** *5,* 379.
[45] C. J. Meledandri, J. K. Stolarczyk, and D. F. Brougham, *ACS Nano* **2011,** *5,* 1747.
[46] L. Wang, H.-Y. Park, S. I. I. Lim, M. J. Schadt, D. Mott, J. Luo, X. Wang, and C.-J. Zhong, *Journal of Materials Chemistry* **2008,** *18,* 2629.
[47] E. Hasmonay, E. Dubois, J.-C. Bacri, R. Perzynski, Y. L. Raikher, and V. I. Stepanov, *Eur. Phys. J. B* **1998,** *5,* 859.
[48] D. Alloyeau, T. Oikawa, J. Nelayah, G. Wang, and C. Ricolleau, *Applied Physics Letters* **2012,** *101,* 121920.
[49] C. Ricolleau, J. Nelayah, T. Oikawa, Y. Kohno, N. Braidy, G. Wang, F. Hue, I. Florea, V. P. Bohnes, and D. Alloyeau, *journal of electron microscopy* **2012,** *62,* 283.
[50] D. Alloyeau, in *Nanoalloys: synthesis, structure and properties*, (Eds: D. Alloyeau, C. Ricolleau, and C. Mottet) Springer, London UK, **2012**, Ch. 4.
[51] C. Langlois, T. Oikawa, P. Bayle-Guillemaud, and C. Ricolleau, *,J. Nanoparticles Research* **2008,** *10,* 997.
[52] D. Alloyeau, C. Ricolleau, C. Mottet, T. Oikawa, C. Langlois, Y. Le Bouar, N. Braidy, and A. Loiseau, *Nature Materials* **2009,** *8,* 940.
[53] D. Alloyeau, C. Ricolleau, T. Oikawa, C. Langlois, Y. Le Bouar, and A. Loiseau, *Ultramicroscopy* **2009,** *109,* 788.

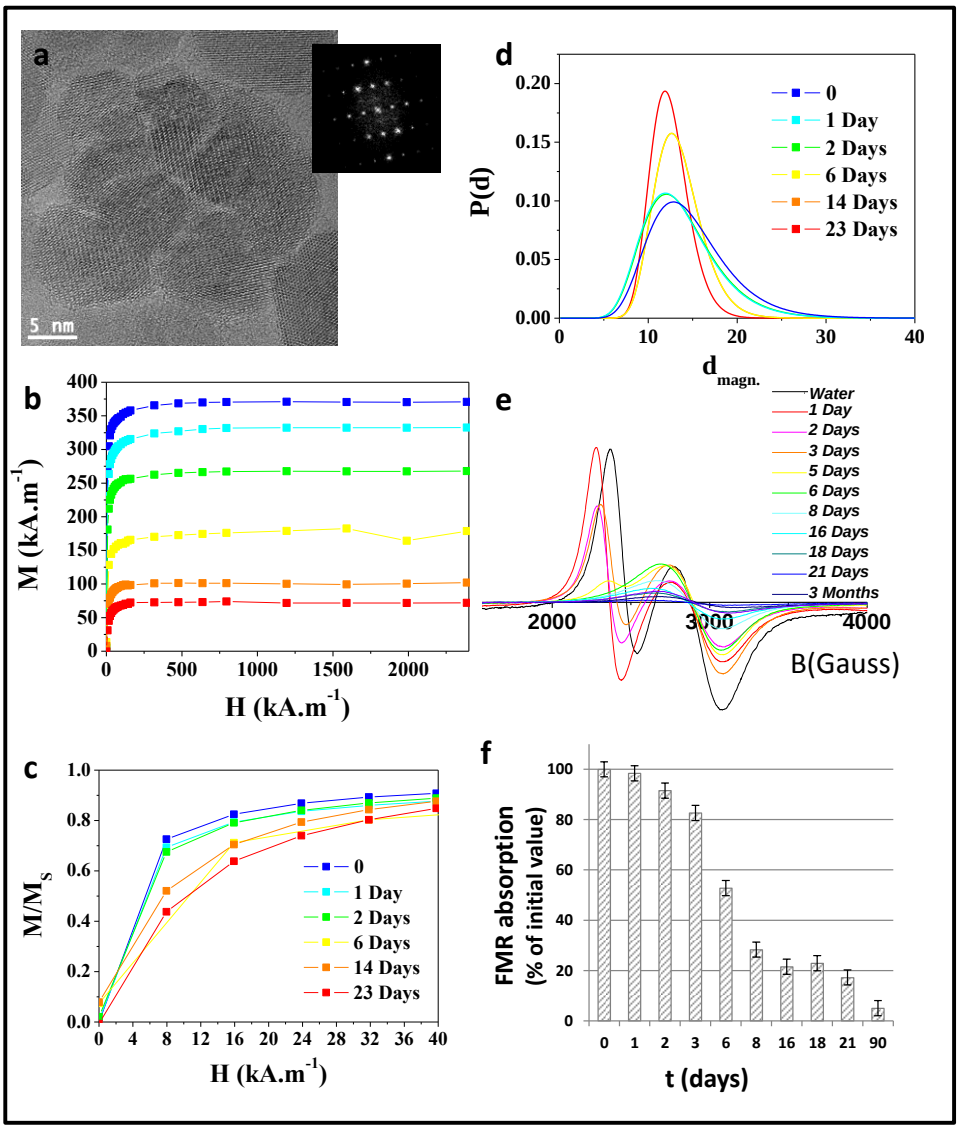

Figure 1: Representative TEM micrograph of the mesoporous multicore nanoflowers (24 nm diameter) synthesized by a polyol method (a). High resolution image and corresponding Fourrier transform (inset) show that NFs are single-crystals composed of smaller maghemite cores sharing a common crystalline orientation. Magnetization measurements demonstrate a deterioration of their magnetic properties when exposed to the lysosome like medium for different times. Both saturation magnetization (b) and initial susceptibility (c) are decreasing over time. The corresponding distribution of apparent magnetic diameter d_{mag} (deduced from the fit of magnetization curves, see supporting information S1) becomes narrower when increasing exposure to the acidic medium (d). Ferromagnetic resonance (FMR) spectrum evolves from the initial multiline shape to a single line spectrum characteristic of single core nanoparticles (e). Quantification of the FMR absorption signal provides the percentage of magnetic iron in a particulate form (f). The loss of magnetic iron in lysosome like medium is well correlated with the diminution of saturation magnetization.

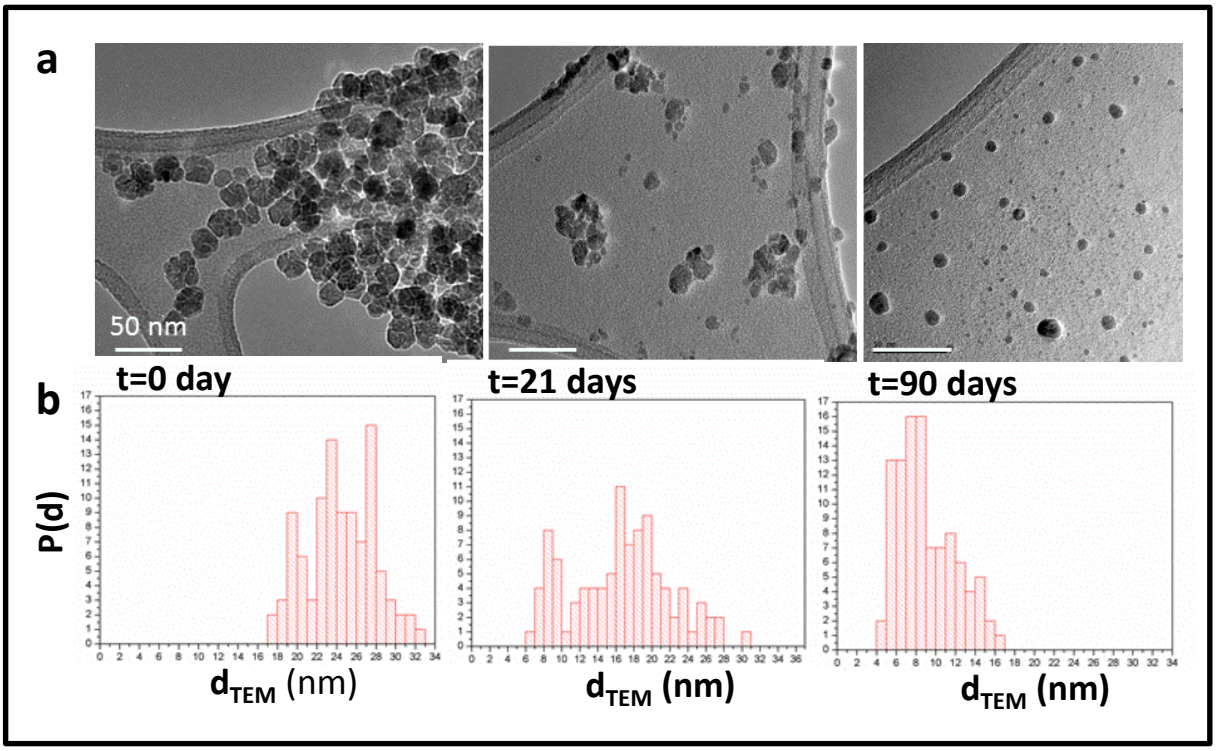

Figure 2: Representative TEM micrograph of nanoflowers at different time points (day 0, day 21, day 90) in the lysosome like medium and corresponding distribution of the TEM particle size (bar is 50 nm).

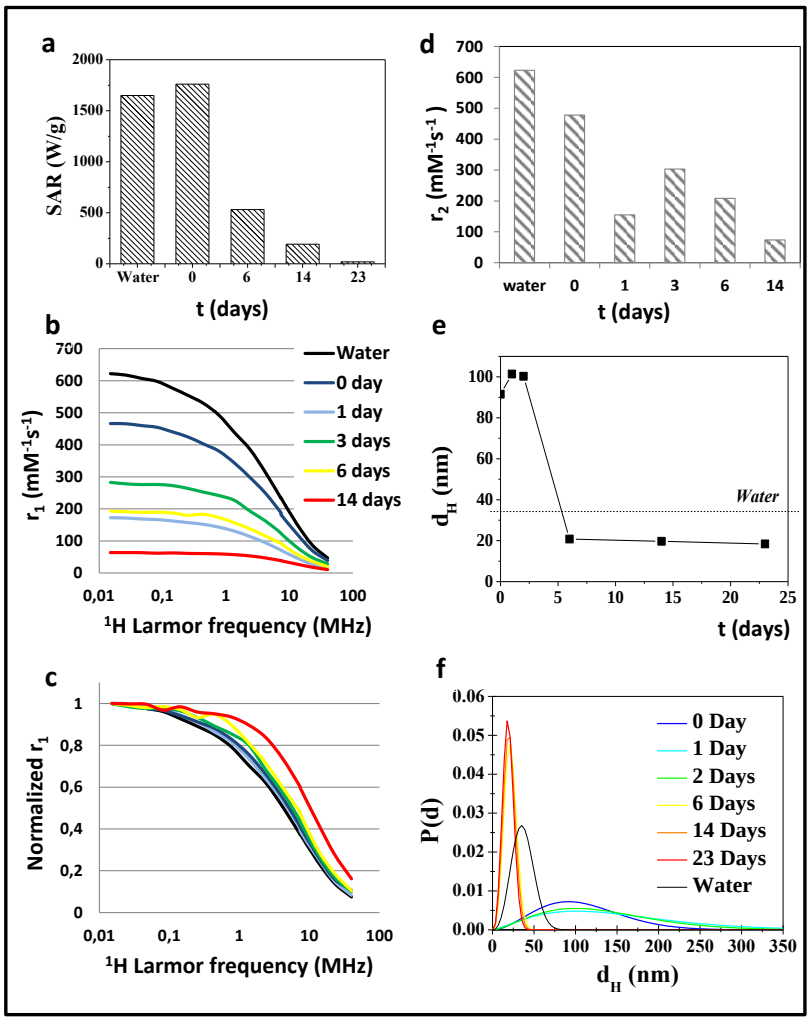

Figure 3: Degradation of nanoflowers in the lysosome like medium impairs their efficiency for magnetically induced hyperthermia and magnetic resonance imaging. The specific absorption rate (SAR) in a magnetic field of 24 kA/m and 520 kHz decreases over time in the acidic medium (a). The NMRD profile of NFs, representing longitudinal relaxivity r_1 as function of the proton Larmor frequency, shows a non-monotonous diminution of relaxometric properties over time (b) and the normalized NMRD profile (normalization by the relaxation rate at 0.015 MHz) is also modified at day 14 (c). The transverse relaxivity r_2 determined at 20 MHz follows the non-monotonous evolution of longitudinal relaxivity (d). To understand such behavior, the distribution of hydrodynamic volumes of NFs was determined from magnetically-induced birefringence experiments. The mean hydrodynamic diameter and the whole distribution of hydrodynamic diameter are represented in (e) and (f), respectively. The initial increase of hydrodynamic volumes reveals the onset of aggregation as soon as citrate-coated NFs are transferred from water to lysosome like medium. The citrate-coated NFs tend to desaggregate from day 3 to day 6 in the lysosomal medium and their mean hydrodynamic volume is reduced to 18 nm indicating the rapid disintegration of the NF structure into single core nanoparticles. We note the parallel evolution of r_1 and r_2 in the lysosome like medium, which first decreases due to

aggregation, then increases at day 3 due to disaggregation and then continuously decrease due to the loss of magnetic iron in the solution. At the longest time, the appearance of a low frequency shoulder in the normalized NMRD profile is indicative of particles with lower magnetic moment and increased rotational mobility (c).

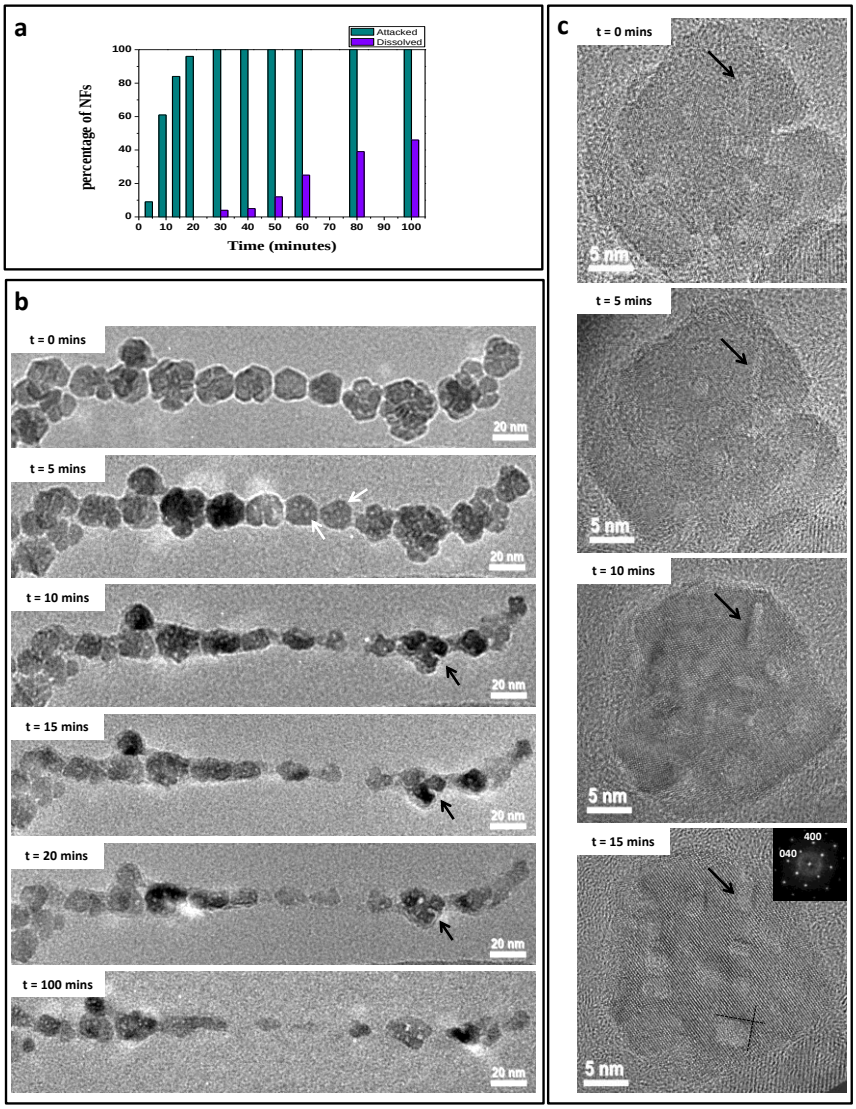

Figure 4: TEM monitoring of NF degradation in a lysosome-like medium. (a) Evolution of the percentage of attacked (green) vs totally dissolved isolated NFs (violet) over time of incubation in the lysosome-like medium (100 NFs were analyzed) (b) Low-resolution TEM monitoring of NFs degradation in the lysosome-like medium (time of incubation is indicated in the top left corners of the images). The NFs which consist in multicore nanoparticles in the initial state are gradually eroded. The white arrows indicate the formation of holes inside the structure (bright spot on the NPs) while the black arrows highlight the slipping process of the multicores

nanostructures. After 100 min in the lysosome-like medium some NFs totally dissolved and only single-core clusters are observed. (c) High-resolution TEM monitoring of the degradation of a single NF in the lysosome-like medium. The black arrows show the milling process of a hole inside the atomic structure of the NF. The holes are formed on defaults (pores) that are observed on the initial NF (t = 0 min). After 15 minutes of immersion the holes present rectangular shapes (indicated by dashed lines) oriented along the [400] and [040] directions of the inverse spinel iron oxide structure here oriented along the [001] zone axis (the FFT of the image in seen in insert).

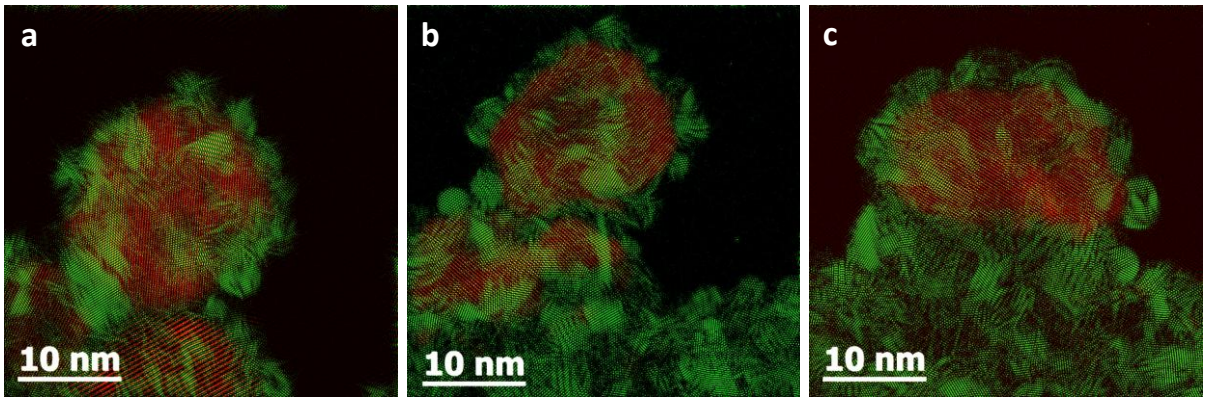

Figure 5: Bragg filtered high resolution images of iron oxide NFs (in red) covered by a gold layer (in green) deposited by PLD technique. The nominal thickness of the gold layer is (a) 3 nm, isolated cluster are formed, (b) 5 nm, a percolated film is formed and (c) 7 nm, a continuous layer is formed.

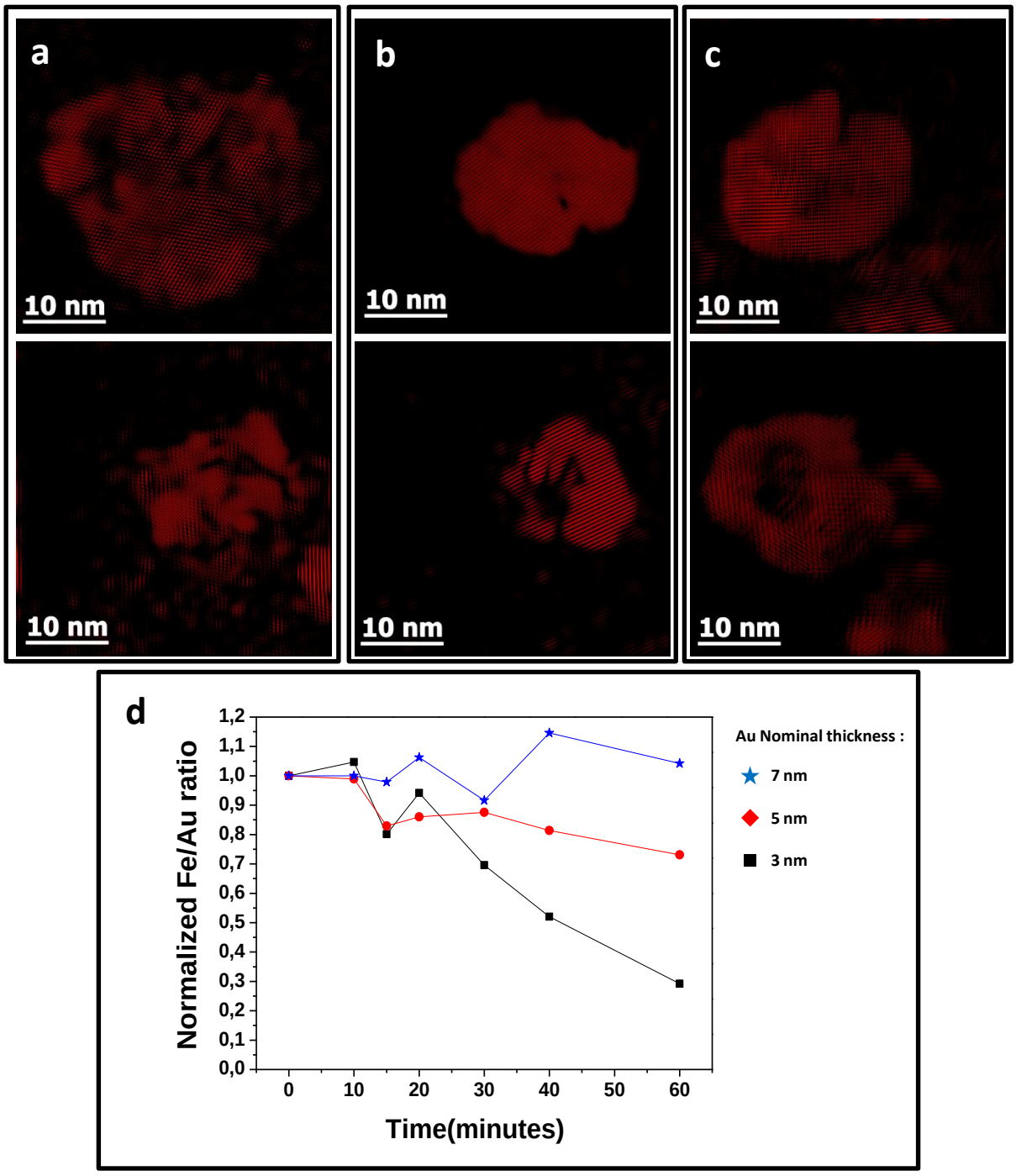

Figure 6: Degradation of iron oxide NFs as a function of the nominal thickness of the protective gold layer. Bragg filtered high resolution images showing only the iron oxide NFs before (top image) and after 45 minutes in the lysosome-like medium (bottom image). The nominal thickness of the gold layer is (a) 3 nm (isolated clusters), (b) 5 nm (percolated film) and (c) 7 nm (continuous layer). (d) EDX quantitative measurement of the Fe/Au ratio in single Au-coated

NFs as a function of the incubation time in the lysosome-like medium. The ratio is normalized by the Fe/Au ratio before incubation (several NPs were individually analyzed on each sample and each data point corresponds to the average of these measurements).

Table 1. Evolution of nanoparticle characteristics over time in the lysosome-like medium.

Time (Days)	**M_S ($A.m^2.kg^{-1}$)**	**d_{mag} (nm) (σ)**	**d_H (nm) (sd)**	**SAR (W/g)**	**d_{NMR} (nm)**
0*	82	14.0 (0.25)	35.0 (0.80)	1604 (56)	22.4
0	71	14.0 (0.30)	91.5 (0.60)	1761 (35)	21.2
1	64	13.0 (0.30)	101.4 (0.44)	-	20.4
2	51	13.2 (0.30)	100.3 (0.46)	-	-
3	-	-	-	-	20.8
6	35	13.1 (0.20)	20.8 (0.90)	532 (58)	20.4
14	19	13.1 (0.19)	19.6 (0.90)	192 (24)	13.2
23	14	12.2 (0.17)	18.4 (0.90)	19 (5)	-

* Measurement realized in water.

TOC figure:

Biodegradation mechanism of iron oxide monocrystalline nanoflowers and tunable shield effect of gold coating

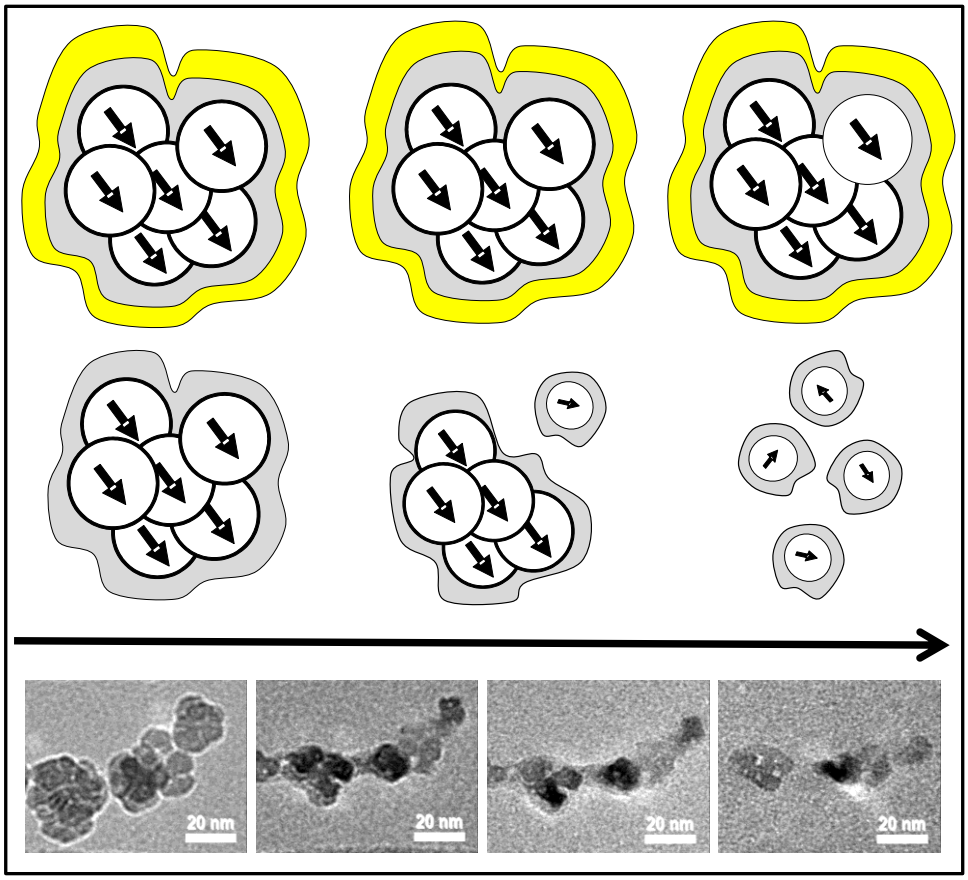

Table of contents entry

By following the magnetic and structural transformations of multicore maghemite nanoflowers in a medium mimicking intracellular lysosomal environment, we have unraveled the mechanisms involved in the critical alterations of their hyperthermic power and their Magnetic Resonance imaging contrast effect. To overcome this harmful influence of cellular medium on the effectiveness of iron oxide-based nanomaterials, we demonstrate that the inert activity of gold nanoshells can be exploited to modulate their degradability.

Supporting Information

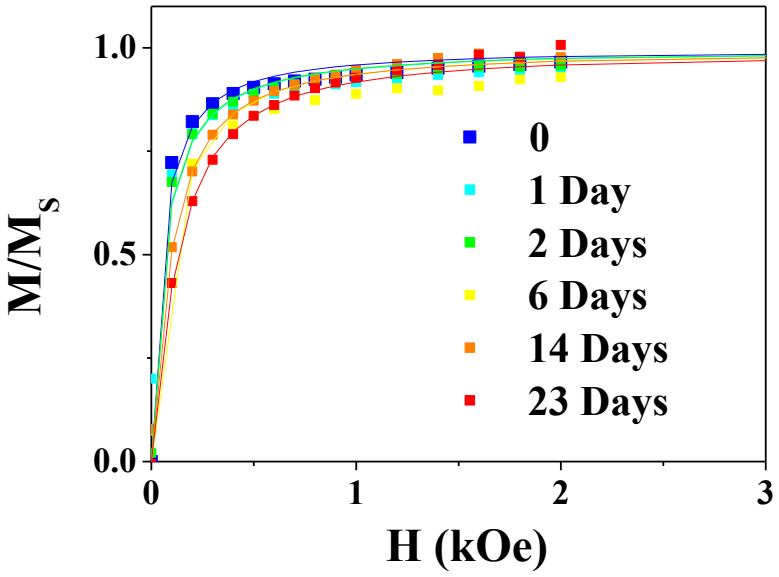

	M_S (kA/m)	χ_0	Fit Langevin (LogNormal)	
			$d_{magn.}$ (nm)	σ
0	367.4	33.6	14.0	0.30
1	329.9	28.3	13.0	0.30
2	268.0	21.7	13.2	0.30
6	174.3	7.2	13.1	0.20
14	101.1	5.3	13.1	0.20
23	71.5	4.0	12.2	0.17

Figure S1: Fit (solid lines) of the magnetization curves of citrate-coated nanoflowers (300K) using a Langevin function weighted by the log-normal distribution of magnetic diameter d_{mag} (polydispersity index σ) displayed in the table. The table also indicates the saturation magnetization M_s and initial susceptibility χ_0 of NFs for different times (in days) in the lysosome-like medium.

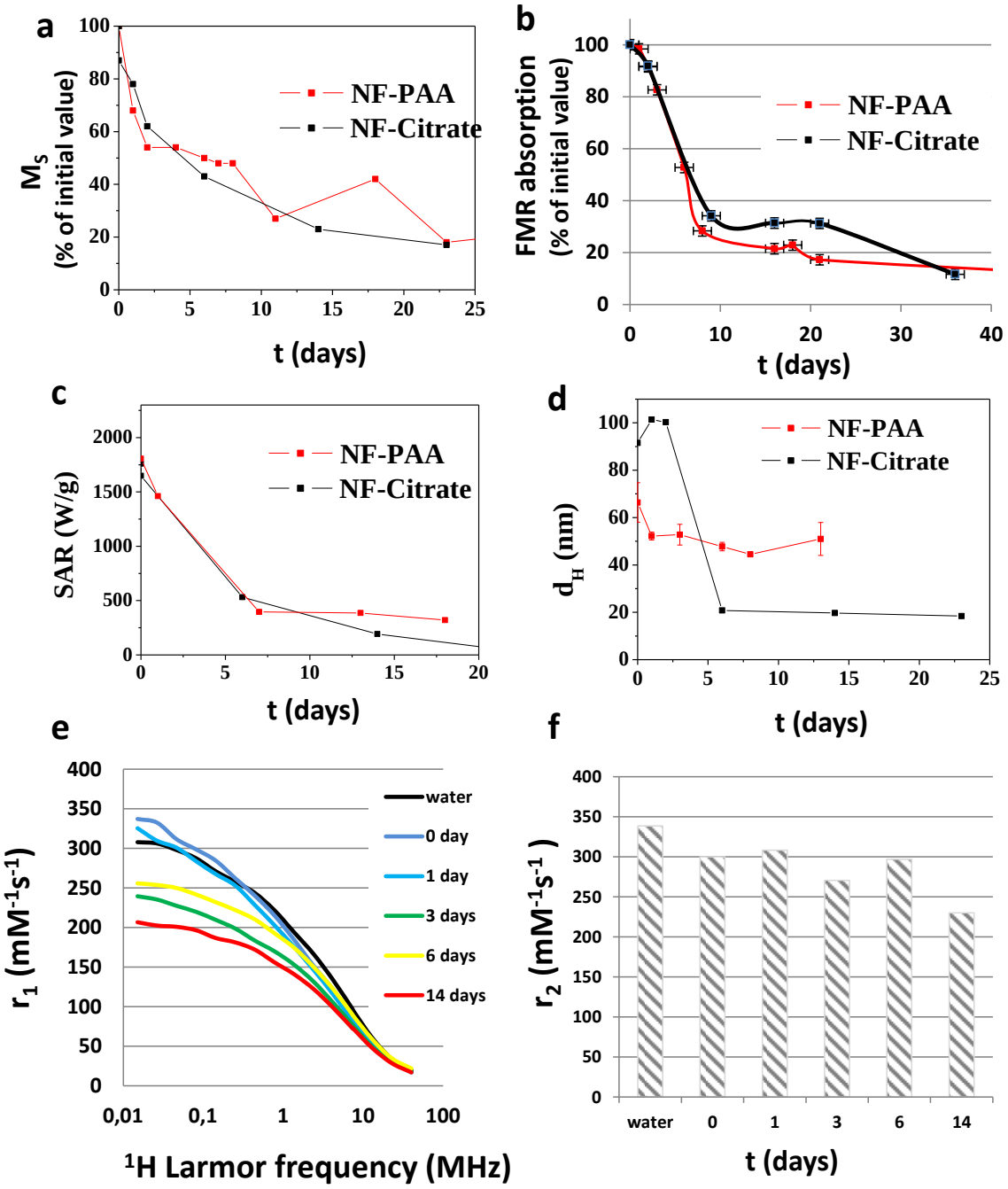

Figure S2: Comparison of magnetic properties of PAA-coated NFs and Citrate-coated NFs in the degradation medium. Evolution of saturation magnetization (a), FMR absorption signal (b), Specific Absorption Rate SAR (c) and hydrodynamic diameter (d) as function of time in the lysosome-like medium. (e) NMRD profile and (f) r_2 relaxivity at 20 MHz of PAA-coated NFs at different time-points.

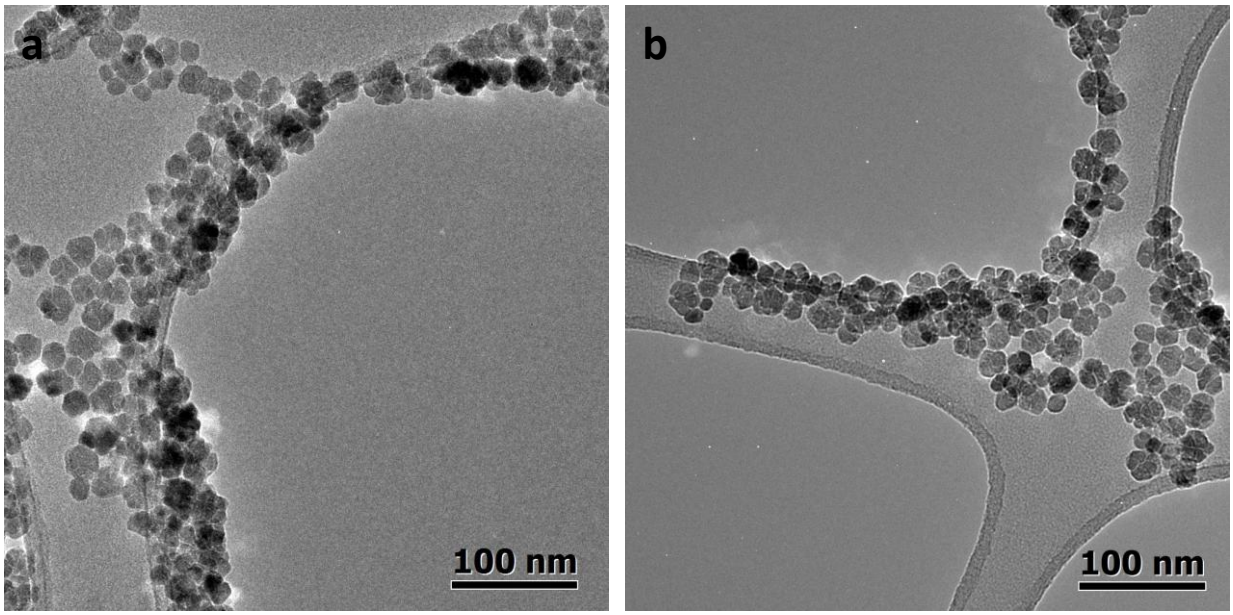

Figure S3: Structural stability of NFs over several months in water. TEM images of NFs (a) just after synthesis, (b) 6 months after synthsis.

The magneto-structural properties of the NFs were firstly studied just after their synthesis. These results were reported in [lartigue et al. *ACS Nano* **2012,** *6,* 10935]. The study of NFs biodegradation reported here started 6 months after the synthesis of the NPs. The close similarities between the magnetic measurements reported in [lartigue et al. *ACS Nano* **2012,** *6,* 10935] and the ones reported here before the insertion of the NFs in the lysosome-like medium (namely in water) demonstrate that the long-term aging of the NFs in water has no impact on their magnetic properties. This result is consistent with the structural stability of the NFs observed by TEM over several months in water (Figure S3). Therefore, the degradation processes observed in the lysosome-like medium allows clearly evaluating the drastic effects of a model biological environment on the structure and properties of iron oxide NFs.

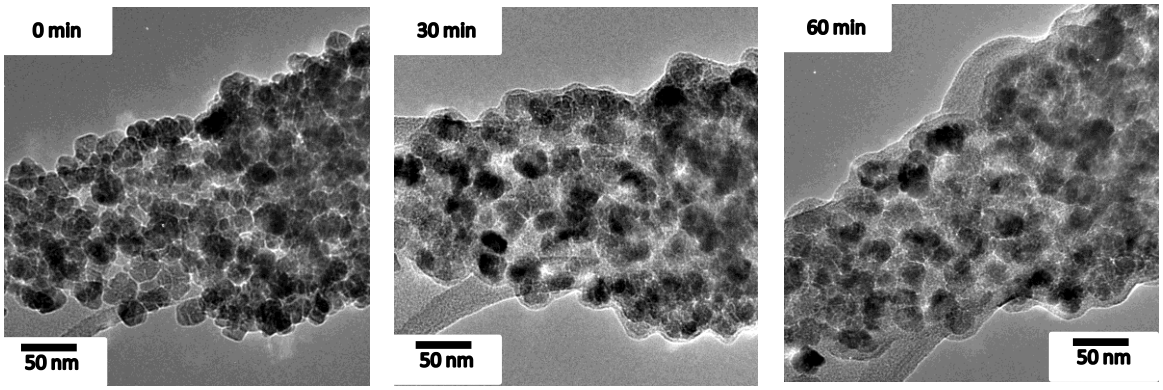

Figure S4: Very slow degradation of a large aggregate of citrate-coated NFs followed by TEM.